PROCESS SIMULATION OF A BOREHOLE THERMAL ENERGY STORAGE COMBINED WITH A REVERSE BRAYTON CYCLE ROTATION HEAT PUMP FOR USE IN DISTRICT HEATING

Matthias Finkenrath[1*], Christian Pressa[1], Verena Jetzinger[1],
Roland Koenigsdorff[2], Fabian Neth[2], Daniel Buchmiller[2]

[1]Kempten University of Applied Sciences, Institute for Energy and Propulsion Technologies, Kempten, Germany

[2]Biberach University of Applied Sciences, Institute of Building and Energy Systems, Biberach, Germany

Corresponding Author: matthias.finkenrath@hs-kempten.de

ABSTRACT

Heat pumps and seasonal thermal energy storage are key technologies for decarbonizing district heating networks. If both are combined, excess heat stored during summer can be very efficiently reused in winter time, even at a raised temperature level. This paper compares two borehole thermal energy storage (BTES) models and introduces a model of an innovative high-temperature heat pump, all of them designed for seamless integration into process simulators. The BTES models are based on an analytical and a numerical simulation approach. They rely on calculating heat transfer rates and temperatures within the borehole depending on the effective borehole resistance and the properties of the surrounding ground. The results of both modeling approaches are compared and validated using long-term operational data from a real ground heat exchanger system. For the heat pump, a reverse Brayton cycle rotation heat pump is modeled, which operates without phase changes and is suitable for temperatures above 100 °C. Pressure and temperature increase are achieved through centrifugal forces. The paper elaborates on the theoretical basis and thermodynamic modeling of this novel heat pump technology. It is demonstrated that the high potential of this heat pump could be effectively utilized in combination with seasonal storage in district heating systems using BTES.

1 INTRODUCTION

District heating networks often generate excess heat during summer, for example from waste incineration or solar thermal collectors. The heat can be stored and reused in winter for heating purposes. To achieve sufficiently high temperature levels, thermal storage can be combined with heat pumps.

Borehole thermal energy storage (BTES) is a widely used technology (see e.g. Kalaiselvam and Parameshwaran, 2014). However, expertise in BTES modeling remains limited to a small group of experts and specialized simulation tools. Moreover, publicly accessible long-term operational data from existing projects - critical for model validation - remains scarce. In many publications dealing with real-life BTES data, the underlying measurement data are either not made publicly available, provide insufficient detail for physical modeling, or pertain to highly specific configurations that may not be widely applicable (e.g., the influence of moving groundwater layers) (Catolico et al., 2016, Andersson et al., 2021, Ramstad et al., 2023, Spitler and Gehlin, 2019, Başer and McCartney, 2020, Lazzarotto, 2021). This lack of accessible data poses a challenge for both research and commercial efforts seeking to assess the potential of BTES in complex energy systems. Such systems often require the integration of multiple energy technologies and sectors, necessitating simplified but accurate BTES models.

In this context, the present paper introduces both an analytical and a numerical modeling approach that enable the seamless integration of BTES models into process simulations. The results of both approaches are compared across different BTES configurations and validated using long-term operational data from a real-world borehole heat exchanger system.

Typically, surplus heat stored in summer in a BTES system cannot be recovered at high temperatures. In such cases, heat pumps are used to raise the temperature to the required supply levels of the district heating network (e.g. Rees, 2016). Reverse Brayton cycle heat pumps are particularly suitable for this purpose, as they operate without phase changes, thereby minimizing exergy losses during heat transfer. In this paper, BTES models are combined with a rotation heat pump model - a novel type of reverse Brayton cycle heat pump that could achieve high operating efficiencies, even at high temperature lifts, through the effective compression of the working fluid via centrifugal forces. Sensitivity analyses of key operating parameters are conducted. Finally, a simplified use case combining BTES with a rotation heat pump is presented to illustrate the potential of this configuration.

All simulation models have been implemented in the process simulation platform EBSILON®Professional.

2 BOREHOLE THERMAL ENERGY STORAGE MODELING

BTES systems utilize the ground as a heat storage medium. In a typical setup, an array of boreholes is drilled to a depth of several tens of meters. Each borehole usually contains one or two U-shaped pipes serving as heat exchangers, with the remaining volume filled with a grouting material. During charging and discharging processes, a heat transfer fluid - such as water - circulates down to the bottom of the borehole and back up.

The arrangement of borehole heat exchangers (BHEs) is often designed to follow a uniform pattern, such as a hexagonal or rectangular grid. For modeling purposes, this allows for the assignment of a specific ground region to each BHE. The fundamental concept of a BTES system is illustrated in Figure 1 below.

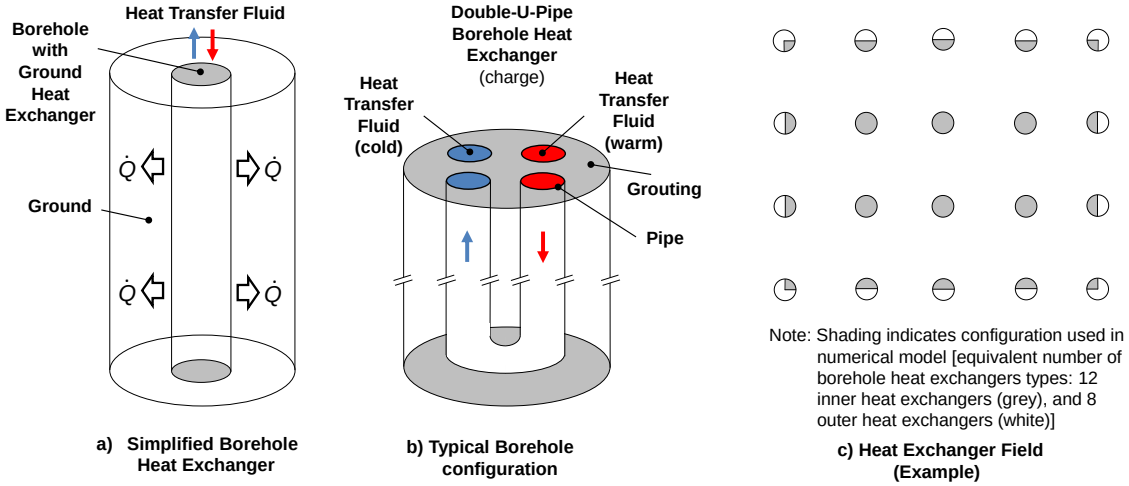

Figure 1: Typical BHE and BTES field configurations.

The overall heat transfer process within a borehole thermal energy storage (BTES) system - encompassing the fluid, pipe material, grouting, and interactions between pipes and the surrounding ground - is characterized by the fluid-to-ground thermal resistance. It is typically referred to as effective borehole thermal resistance, $R_{\mathrm{b,eff}}$. It serves as the fundamental parameter for both the analytical and numerical BTES models analyzed in this study, as illustrated in Figure 2.

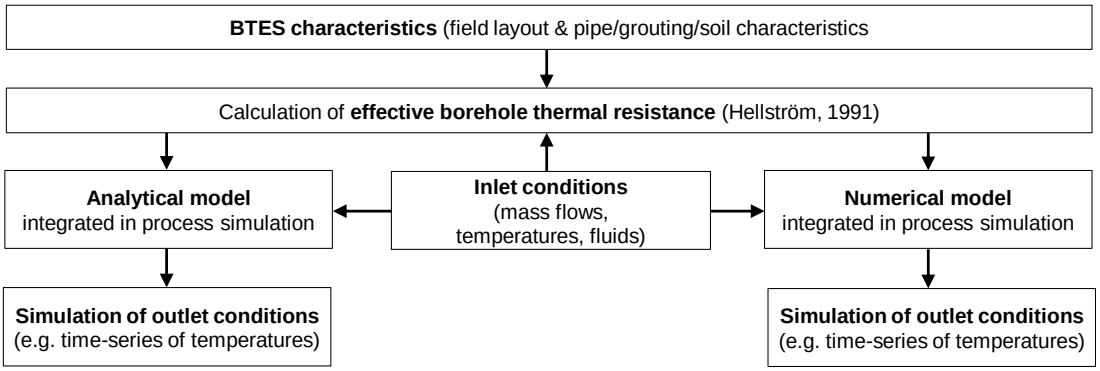

Figure 2: Comparison of BTES modeling approaches.

The key components contributing to $R_{\mathrm{b,eff}}$ include:

- the convective thermal resistance between the fluid and the pipe wall, R_{α},
- the thermal resistance of the duct/pipe wall, R'_{p},
- the contact resistance at the interface between the duct/pipe wall and the surrounding material, R_{c}, which is typically negligible,
- the thermal resistance between the pipes and the ground, R_{b},
- the thermal resistance between individual pipes, R_{a},
- the thermal capacity flow and borehole length (together with R_{a}, both govern the thermal short-circuit effect between upflow and downflow pipes in the borehole).

The complete calculation of $R_{b,eff}$ is extensive. A detailed explanation and a simplified modeling concept - applied in this paper - are provided in Hellström, 1991. In this approach, flow channels are approximated as line sources, and average temperatures for the fluid and borehole wall (T_f, T_b) are assumed over the entire borehole length.

2.1 Analytical model

In the analytical BTES model, the temperature at the borehole wall is determined using so-called *g-functions*, which describe the time-dependent, dimensionless thermal response of a corresponding BHE field (Eskilson, 1987). The model is based on the principle that, depending on the injected or extracted heat flux, the temperature change between the undisturbed ground and the borehole wall can be spatially superimposed and accumulated over time, starting from the initial ground temperature. The thermal influence of past heat injections or extractions is accounted for by the superposition of *g-function* values.

In this study, the Python tool *pygfunction* is used to compute *g-functions* (Cimmino, 2015, Cimmino, 2018). It is is an open-source, free-to-use software that integrates well with the presented approach, which is also implemented in the Python programming language. Using *pygfunction*, it is possible to calculate *g-functions* for different boundary conditions, including the specified inlet temperature boundary condition required in this work (Cimmino, 2019, Cimmino and Cook, 2022).

The analytical model and its implementation into a commercial process simulation environment, as applied in this paper, have been described in detail in Neth et al., 2024 and Pressa et al., 2024.

2.2 Numerical model

The numerical model of a single borehole heat exchanger (BHE) represents a cylindrical pipe that facilitates heat transfer and storage to the surrounding pipe wall, which corresponds to the ground in a BTES application, as illustrated in Figure 1a). The model calculates the transient heat exchange between the fluid flowing through the pipe and the surrounding materials (borehole backfilling and surrounding ground).

This numerical model is based on a standard component available in many process simulators (e.g., in EBSILON®Professional: component 119 ”indirect storage”). Using a two-dimensional Crank-Nicolson algorithm, the transient heat transfer equation for the ground is discretized and solved numerically. The resulting solution provides a temperature field within the storage wall. To maintain the assumption of uniform fluid and borehole wall temperatures, discretization is applied only in the radial direction.

An equivalent heat transfer coefficient from the fluid to the surrounding ground is derived based on the effective borehole thermal resistance, $R_{b,eff}$. The numerical model must be adapted to approximate real BTES configurations involving multiple BHEs, as these are subject to varying boundary conditions. As shown in Figure 1c), BHEs located inside the BTES field, and those parts of them facing to the inside, experience approximately adiabatic boundary conditions due to the symmetry of the temperature fields (gray areas). In contrast, those parts facing to the outside area (white areas) are subject to heat transfer to an infinite surrounding ground region.

In the simulation, results from the models representing inner and outer BHEs are combined after the simulation, weighted by the equivalent number of BHEs in each configuration. For the example in Figure 1c), the equivalent distribution includes 12 inner heat exchangers (summarized gray areas) and 8 outer heat exchangers (summarized white areas). To account for the difference in geometry, where the model represents a cylindrical pipe but the inner BHEs are assigned a rectangular ground region, the associated mass for each BHE is adjusted accordingly.

2.3 Model validation

The analytical and numerical models were compared using a test case representing a rectangular 17x17 BHE field with double U-shaped heat exchangers. The simulated outlet temperatures and corresponding average heat fluxes per BHE for this 17x17 test case are presented in Figure 3. At the beginning of each load change, the simulation shows high peak heat fluxes per BHE. This is due to the significant instantaneous temperature differences that occur when a fluid with a sudden temperature change enters during the transition between charging and discharging, or vice versa.

For the comparison, a test case with alternating charging (at 85 °C) and discharging phases (at 35 °C) was selected. Over a simulated period of five years with hourly time steps, deviations between the numerical model results and the measured data were on average 0.8 K in temperature (mean absolute error, MAE) and 4.7 % for the total energy transferred.

Additionally, for a single BHE test case (1x1; not included in this publication), average deviations between numerical and analytical models were 0.8 K in temperature (MAE) and 5.2 % for the total energy transferred.

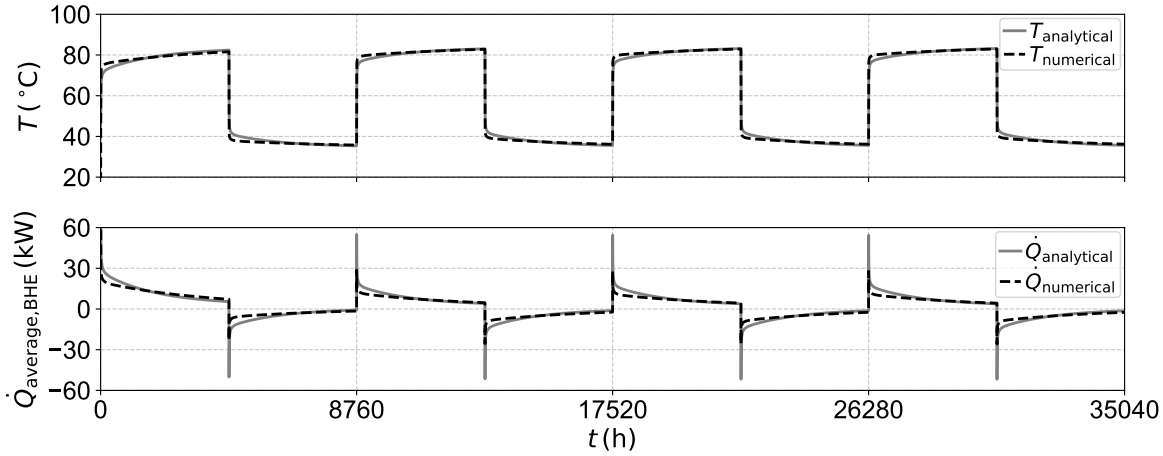

Figure 3: Comparison of modeling approaches for a 17x17 rectangular double-U-pipe BTES

Furthermore, the numerical model was validated against real-world operational data from a BHE field at the Hugh Aston building of De Montfort University. This field comprises two borehole arrays containing 19 and 37 single U-shaped BHEs (Naicker and Rees, 2018, Naicker and Rees, 2020). Measurement data for the De Montfort University BHE system were recorded at a one-minute resolution. For the simulation, these data were averaged to 15-minute intervals.

Figure 4 compares the simulated outlet temperatures and corresponding heat fluxes with the measured data from 2011 for the BHE system. Deviations between the numerical model results and the measured data were on average 0.9 K in temperature (MAE) and 1.2 % for the total energy transferred.

Table 1 summarizes the parameter settings assumed for both the test case and the real BHE field.

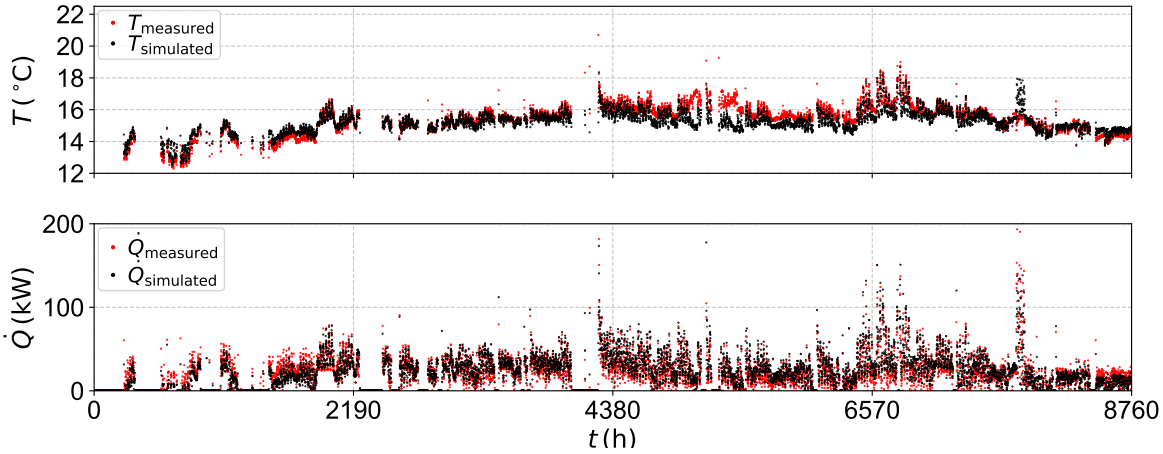

Figure 4: Validation of numerical model against De Montfort University BHE data.

3 HEAT PUMP MODELING

Heat pumps are used in district heating networks to raise temperatures to the required supply levels. This is particularly crucial for high-temperature applications, as many existing district heating networks still operate at temperatures of 120 °C or higher. In such cases, achieving a high coefficient of performance (COP) despite of the high temperature needed is essential. A comprehensive overview of available high-temperature heat pump technologies is provided by Arpagaus et al., 2018. For high-temperature applications, heat pumps based on a reverse Brayton cycle offer several advantages. Since the working fluid remains in a gaseous state throughout the process, heat can be absorbed and released with minimal exergetic losses from sensible heat sources or sinks - such as water - which are commonly used in district heating applications. The potential advantage of a reverse Brayton

Table 1: Parameters of simulated BHE systems.

Simulated case	**1x1 test case**	**17x17 test case**	**De Montfort Univ.**
Number of BHE	1	289	56
Configuration	rectangular	rectangular	rectangular
BHE type	Double-U	Double-U	Single-U
Depth of BHE (m)	55	70	100
Distance between boreholes (m)	–	4	5
Borehole diameter (m)	0.15	0.15	0.125
Pipe material	PEX	PEX	HDPE
Outer pipe diameter (m)	0.032	0.032	0.032
Pipe thickness (m)	0.003	0.003	0.004
Spacing between pipe centers (m)	0.08	0.08	0.093
Thermal conductivity (pipe) (W/(mK))	0.38	0.38	0.4
Thermal conductivity (grouting) (W/(mK))	2	2	0.66
Thermal conductivity (ground) (W/(mK))	2.5	2.5	3.45
Density (ground) (kg/m^3)	2500	2500	1650
Specific heat capacity (ground) (kJ/(kgK))	960	960	1681
Typical mass flow per BHE (kg/s)	0.5	0.5	0.2
Effective borehole thermal resistance ((Km)/W)	0.057	0.057	0.186

cycle heat pump compared to a standard reverse Rankine cycle heat pump is illustrated in the T-s-diagram on the left side of Figure 5.

Moreover, reverse Brayton cycle heat pumps can utilize working fluids that are non-toxic, non-flammable, free from per- and polyfluoroalkyl substances (PFAS), and have no greenhouse gas or ozone depletion potential. They also offer greater adaptability to fluctuating heat source and heat sink temperature levels - conditions that frequently occur when charging or discharging BTES systems, and in district heating networks during seasonal variations.

3.1 Rotation heat pump concept

In order to deliver heat at the raised supply temperature level of typical existing heating networks efficiently, the innovative technology of a rotation heat pump is considered. This type of heat pump works according to a reverse Brayton cycle. Fundamentally, the working fluid is compressed by centrifugal forces generated through rotation around an axis. The underlying principle of rotation heat pumps was first introduced in the 1970s (Los and Wind, 1976, Leidenfrost and Eisele, 1972) and has been revisited sporadically in subsequent years (Nowacki and Granryd, 1998).

The most advanced concept, which has reached commercial viability and incorporates critical features - such as the use of a noble gas working fluid circulating in a closed loop - was first described in patent applications related to Adler, 2009. The main cycle steps of the rotation heat pump include reversible, adiabatic compression and expansion achieved through the rotation of a closed working fluid loop around an axis, combined with isobaric heat addition and rejection, as illustrated in Figure 5 on the right side.

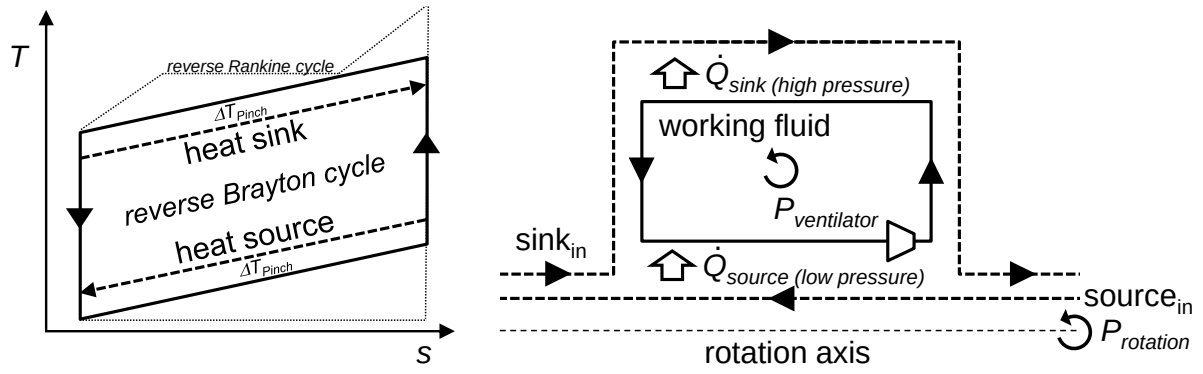

Figure 5: T-s diagram of reverse Brayton cycle heat pump (left) and rotation heat pump working principle (right).

A ventilation fan is used to overcome pipe frictional losses in the system. Additionally, the fan regulates the working fluid mass flow within the closed cycle, thereby controlling the thermal power transfer capacity. During operation, the pressure - and consequently the temperature - at the heat sink can be adjusted by varying the rotational speed.

Typical working fluids for the system include high-density noble gases such as krypton, argon, and xenon, or mixtures thereof. Unlike turbo compressors, the system operates at relatively low flow velocities, which significantly differentiates its performance characteristics.

Apart from publications by the developers, limited independent analyses of this concept are available in the open literature. For instance, Karlsen and Dong, 2015 examined a similar concept but without considering a closed-loop working fluid circuit. The concept has since undergone continuous development (e.g. Adler and Mauthner, 2016) and experimental validation (Längauer et al., 2020). Recent design advancements focus on enhancing operational flexibility, compactness, heat transfer efficiency, and achieving higher operating pressures through increased rotational speeds (Zotter et al., 2024).

3.2 Fundamentals

The radial pressure gradient of a compressible gas in a rotating system arises due to the centrifugal force, as described by Eq. 1:

$$\frac{dp}{dr} = \rho(p,T)\omega^2 r \tag{1}$$

where:

- $\rho(p,T)$: Density, as a function of the local pressure and temperature (that depend on the rotation radius and angular velocity, and compression/expansion efficiency),
- ω: Angular velocity,
- r: Radial distance.

Unlike the hydrostatic pressure distribution in liquids, the compression of gases can result in significant density changes. Due to the compressibility of the working fluid, an energy difference may arise between the compression and expansion phases. In thermodynamics, the pressure-change work is represented by the integral $\int \frac{1}{\rho}\, dp$, which characterizes how the specific volume changes with pressure. The required pressure-change work was calculated for both the compression and expansion phases under the assumption of isentropic state changes. However, the difference was found to be less than 0.5 %, and thus this effect was considered negligible.

This analysis assumes steady-state conditions. During system startup or significant load changes, the system must be accelerated to its operating speed. Approximating the rotating part as a cylindrical rotor - similar to a flywheel - the rotational kinetic energy (E) can be expressed by Eq. 2, as described in Bolund et al., 2007:

$$E = \frac{1}{4} m r^2 \omega^2 \tag{2}$$

The overall energy required to repeatedly accelerate the system throughout the year could be accounted for, for instance, in a yearly performance factor. However, to a large extent, the energy stored in the rotational mass could likely be recovered during the system's ramp-down phase.

The theoretical energy required to accelerate the rotor is relatively small. For example, accelerating a cylindrical mass of 5 tons with a radius of 1 m to an angular velocity of ω = 150 rad/s requires approximately 28.1 MJ. This corresponds to an average power consumption of 7.8 kW, if the acceleration occurs within 1 hour. Since the energy required for rotor acceleration is minimal compared to the thermal power levels considered in this study (700 kW_{th}), it is deemed negligible and, therefore, excluded from further analysis.

3.3 Assumption for simulations

This paper aims to quantify the fundamental potential of rotation heat pump technology under optimal conditions. Similar to the study presented by Zotter et al., 2024, krypton (R784) is used as the working fluid. In the pressure and temperature ranges of interest, density deviations from ideal gas behavior can reach up to 25 %. Therefore, the reference equation of state for krypton, as implemented in *RefProp* (Lemmon et al., 2018), is utilized to ensure accurate thermodynamic property calculations.

To minimize exergetic losses during heat transfer, the approach temperature between the working fluid and both the heat source and sink fluids is maintained constant within the heat exchangers. This is achieved by adjusting the mass flows of the heat source and sink fluids such that the heat capacity flows ($\dot{m} \cdot c_p$) are kept equal.

For a thermal power output of P_{th} = 700 kW supplied to the heat sink, with a temperature lift of ΔT= 40 °C, the corresponding typical mass flow rates of the working fluid, krypton, range between 40-50 kg/s.

Other thermodynamic assumptions are derived from published data (e.g. Zotter et al., 2024, Adler et al., 2011):

- isentropic compression and expansion efficiency of $\eta_{\text{compr./exp.}}$ = 99 %
- isentropic efficiency of $\eta_{\text{ventilator}}$ = 87 %
- approach temperatures in heat exchangers ΔT_{pinch}= 5 K
- starting pressure p_{low} = 100 bar
- thermal power supplied to heat sink P_{th} = 700 kW
- low flow velocities $v \approx$ 10 m/s (depending on selected flow channel geometries and operating regime)
- typical angular velocity $\omega \approx$ 150 rad/s (varying depending on desired operating pressures)

As stated above, the developers of the rotation heat pump claim exceptionally high isentropic compression and expansion efficiencies, attributed to the low flow velocities of approximately 10 m/s (Adler et al., 2011). To validate this claim, detailed fluid dynamic calculations (based on specific design data) or experimental measurements would be required. However, as no specific design is available in this study, such experimental work or computational fluid dynamics (CFD) calculations were beyond the scope of this analysis. In order to assess the impact of these parameters, sensitivity analyses of key assumptions - particularly those related to isentropic compression and expansion efficiencies - are conducted and presented in the simulation results section.

Adiabatic compression and expansion are assumed in this study. The heat pump typically operates in a vacuum to minimize friction losses caused by air drag; thus, heat losses to the ambient are primarily limited to radiation and are considered negligible. Pressure losses were typically maintained below 5 bar across the analyzed operating regimes.

Geometric parameters of the piping system are estimated based on figures from published sources. The heat sink and heat source heat exchangers are assumed to rotate at a radial distance of 1 m from the axis of rotation. It is further assumed that the fluid is distributed across 100 flow channels in both the heat sink and source heat exchangers, with channel diameters of 1 cm each and a length of 1 m (for each the heat sink heat exchanger, heat source heat exchanger, and interconnecting flow paths). In this configuration, the average flow velocity was calculated to be 20 m/s or lower, based on the mass flow relative to the cross-sectional area. In practice, due to radial acceleration and Coriolis forces within the system, local velocity variations, uneven flow distributions, and the presence of secondary flows are expected. These phenomena could be further investigated through CFD analysis.

The flow within the working fluid channels is highly turbulent. Pressure losses in hydraulically smooth flow channels under turbulent conditions are calculated based on the flow velocity v, pipe diameter D and pipe length l by Eq. 3, as described in Štejnberg and Idelčik, 2008:

$$\Delta p_{\text{pipe}} = f \frac{L}{D} \rho \frac{v_{\text{pipe}}^2}{.} \tag{3}$$

The friction factor f is calculated using Hagen-Poiseuille, Blasius, or Nikuradse approximations, depending on the Reynolds number, as described in the same reference. For turbulent flows, pressure losses in fittings such as bends or junctions are estimated using Eq. 4:

$$\Delta p_{\text{bending/splitting/merging}} = K \rho \frac{v^2}{2} \tag{4}$$

The loss coefficient K depends on the system geometry. Since detailed design parameters were not available, conservative (upper-bound) estimates were used, representing typical values for disadvantageous conditions such as small bending diameters (R/d). Accordingly, the loss coefficients were estimated as $K \approx 0.5$ for bends and $K \approx 1$ for abrupt expansions and contractions occurring before and after the assumed single fan. Due to the significant density variations along the flow path, pressure losses were calculated separately for the low- and high-pressure sides of the working fluid circuit.

Accurately estimating various losses associated with air and mechanical friction, power electronics, and vacuum

pump operation presents a challenge. To address this, an analogy to steel-based flywheel energy storage systems - due to their similar design and operational principles - is considered. Reported efficiencies of flywheel energy storage systems in the literature range from less than 1 % during steady-state operation (Li and Palazzolo, 2022) to overall efficiencies of 91-95 % for large systems (Bolund et al., 2007) and roundtrip energy efficiencies in the range of 90-95 % (Chen et al., 2009). As a conservative assumption, an overall efficiency of 90 % is adopted in this study to account for the aforementioned effects.

Based on the assumptions outlined in this section, the performance calculation presented by Zotter et al., 2024 for an operating point with a heat source temperature of 100 °C and a heat sink outlet temperature of 200 °C is closely matched, yielding a calculated COP of 3.4 compared to the reported value of 3.5 in the publication.

3.4 Simulation results

Based on these assumptions, a sensitivity analysis was conducted for the rotation heat pump technology. Figure 6 illustrates the impact of the following key parameters for different source temperatures:

a) the impact of the isentropic compression and expansion efficiency $\eta_{\text{compr./exp.}}$ on the COP
b) the impact of the isentropic ventilator efficiency $\eta_{\text{ventilator}}$ on the COP
c) the impact of the initial pressure p_{low} on the COP
d) the impact of the initial pressure p_{low} on the maximum pressure p_{max} reached by the working fluid on the high-pressure side of the cycle

Unless otherwise specified, all parameters are based on the previously outlined assumptions. In all analyzed cases shown in Figure 6, the heat sink fluid is heated by 40 °C, reaching an outlet temperature of 130 °C. Considering a pinch temperatur of 5 °C in the heat exchanger as specified under the assumptions before, this requires a heat pump working fluid temperature lift up to 135 °C.

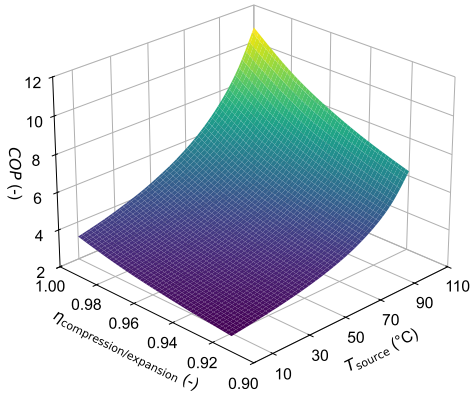

(a) Impact of $\eta_{\text{compr./exp.}}$ on COP

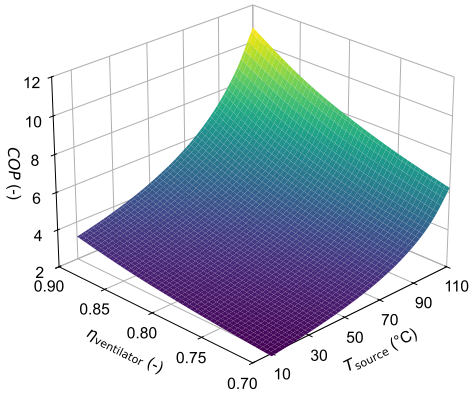

(b) Impact of $\eta_{\text{ventilator}}$ on COP

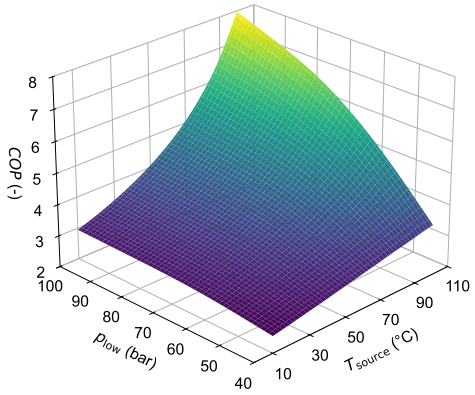

(c) Impact of p_{low} on COP

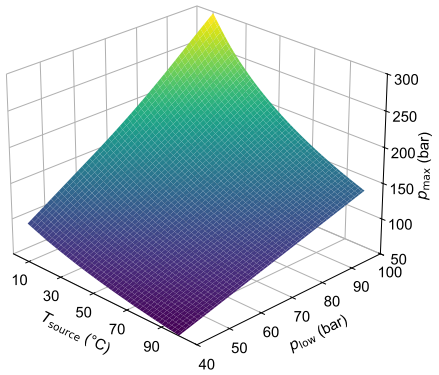

(d) Impact of p_{low} on p_{max}

Figure 6: Simulation results for COP and p_{max} ($T_{\text{sink,out}}$ = 130 °C) for different source temperatures.

The data indicate a high theoretical performance potential of the rotation heat pump concept. As expected, higher source temperatures generally lead to higher COP values, since a lower temperature lift is required from the heat

pump in such cases. However, the simulation results highlight the critical importance of achieving high isentropic compression and expansion efficiencies to attain high COP values. In contrast, the impact of the ventilator's isentropic efficiency on overall performance is lower, as it only needs to overcome the relatively low pressure losses within the working fluid loop compared to the overall pressure ratio.

With fixed working fluid channel geometries as described earlier, higher COPs can be achieved by increasing the initial pressure p_{low}. These effects become more pronounced at higher heat source temperatures due to the increasing divergence of the fluid's isobars at elevated temperatures. However, selecting excessively high initial (lower) pressures results in significantly elevated maximum pressure levels at high temperature lifts. This would also lead to high required annular velocities. These are in the range of approximately 150 rad/s (about 25 Hz) for pressure increases of 50 bar, but would need to reach nearly 250 rad/s (around 40 Hz) for pressure increases of 100 bar within the working fluid loop.

Figure 7 presents performance trends for various heat source temperatures and temperature lifts (i.e., different heat sink temperatures). In all cases, the heat sink fluid is heated up by 40 °C. For this analysis, a lower initial pressure of p_{low} = 80 bar was selected as a compromise to achieve good performance (as indicated in Figure 6, subplot c)), while avoiding excessively high pressures on the high-pressure side. All other parameters are based on the assumptions outlined earlier.

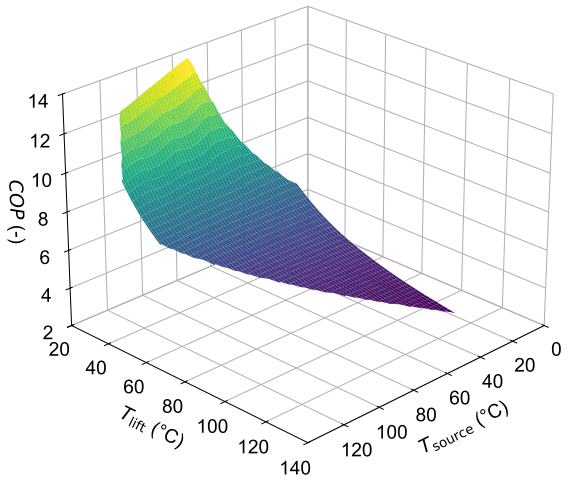

Figure 7: Impact of T_{source} and T_{lift} on COP (with p_{low} = 80 bar, $\eta_{\text{compr./exp.}}$ = 99 %)

4 COMBINED BTES AND HEAT PUMP SIMULATION

In a final test case, the numerical BTES model and the rotation heat pump model were integrated. The BTES model was configured to match the De Montfort University BHE system (see Table 1). The heat pump was utilized to elevate the BTES outlet temperature to a heat sink level of 130 °C. Figure 8 presents the simulation results.

Since the De Montfort University system operates at relatively low temperatures, alternating charging (at 85 °C) and discharging temperatures (at 35 °C), similar to the 17x17 test case, were imposed. The initial ground temperature was set to 10 °C.

The upper subplot in Figure 8 displays the simulated temperatures at the BTES inlet ($T_{\text{in,BTES}}$), outlet ($T_{\text{in,BTES}}$) and the average ground temperature ($T_{\text{average,BTES}}$). The lower subplot shows the COP achieved by the heat pump and the thermal power supplied to the heat sink $\dot{Q}$.

Under the given assumptions, the system achieves COP values of 3 or higher, despite the significant temperature lift from approximately 35 °C to 135 °C (considering approach temperatures).

4.1 CONCLUSIONS

An analytical and a numerical BTES model have been developed and successfully integrated into a process simulation environment. Despite their simplified modeling approaches, both models demonstrate good agreement when compared with each other and with operational data from a real BHE system. It is planned to extend the validation also to data from BTES systems.

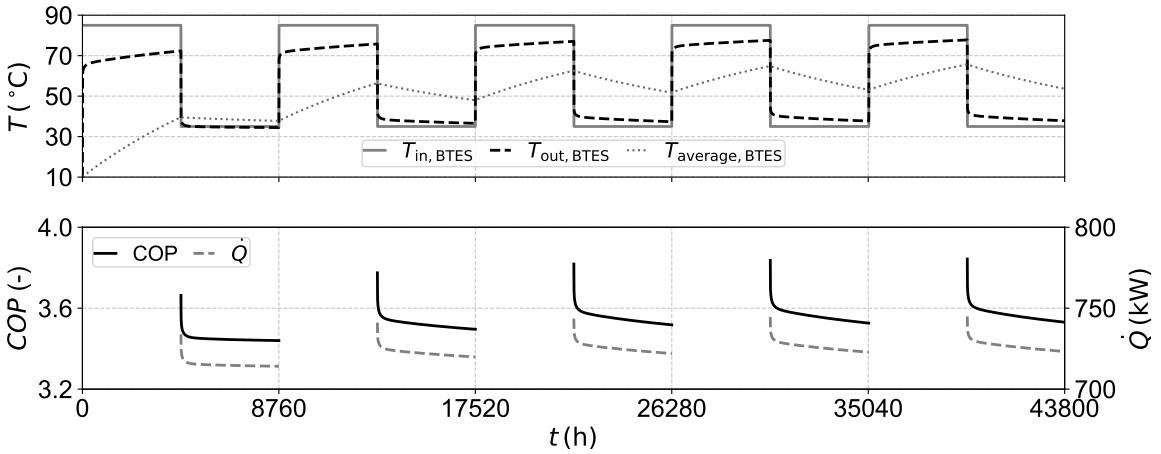

Figure 8: Combined BTES and heat pump simulation case.

Additionally, a model for the rotation heat pump - an innovative reverse Brayton cycle heat pump that utilizes centrifugal forces to efficiently pressurize a working fluid in a closed loop - was developed. This model enables sensitivity analyses of key process parameters, such as flow channel design for minimizing pressure losses and initial pressure levels. The modeling results indicate that the rotation heat pump has significant potential to achieve highly favorable COPs, provided that compression and expansion processes can be realized in a near-isentropic manner.

When combined with a BTES system, the heat pump can achieve high COPs even at substantial temperature lifts.

The developed models can be further utilized for future process simulations, such as front-end engineering and design studies, or for optimizing individual and combined system components. For the heat pump, a more in-depth assessment using computational fluid dynamics (CFD) analysis and experimental validation would be beneficial to confirm the findings of this study. Regarding the thermal energy storage model, the validation process is planned to be extended to include data from a real BTES system.

NOMENCLATURE

Abbreviations

BHE	Borehole heat exchanger
BTES	Borehole thermal energy storage
CFD	Computational fluid dynamics
COP	Coefficient of performance
MAE	Mean absolute error
PFAS	Per- and polyfluoroalkyl substances

Latin Symbols

D	Diameter, m
E	Energy, J
f	Friction factor
K	Loss coefficient
L	Length, m
m	Mass, kg
p	Pressure, bar
r	Radial distance, m
R	Borehole thermal resistance, Km/W
T	Temperature, °C
v	Velocity, m/s

Greek Symbols

Δ	Difference
ρ	Density, kg/m^3
ω	Angular velocity, rad/s

Superscripts and Subscripts

α	convective heat transfer coefficient, W/m^{2}K
b	borehole
c	contact
eff	effective
f	fluid
low	lower
max	maximum
p	pipe

REFERENCES

Adler, B. (2009). *Method for converting thermal energy at a low temperature into thermal energy at a relatively high temperature by means of mechanical energy, and vice versa* (WO2009015402 (A1)).

Adler, B., & Mauthner, R. (2016). https://permalink.obvsg.at/AC12517372

Adler, B., Riepel, S., & Ponweiser, K. (2011). Centrifugal compression turbo heat pump made by ecop. *10th Heat Pump Conference 2011, 16 - 19 May 2011, Tokyo, Japan*.

Andersson, O., Rydell, L., & Håkansson, N. (2021). IEA Annex 52 - Case study report for the Xylem HT-BTES plant in Emmaboda, Sweden. Efficiency by using heat pumps for extraction of stored heat. https://doi.org/10.23697/j2hk-4x61

Arpagaus, C., Bless, F., Uhlmann, M., Schiffmann, J., & Bertsch, S. S. (2018). High temperature heat pumps: Market overview, state of the art, research status, refrigerants, and application potentials. *Energy*, *152*, 985–1010. https://doi.org/10.1016/j.energy.2018.03.166

Başer, T., & McCartney, J. S. (2020). Transient evaluation of a soil-borehole thermal energy storage system. *Renewable Energy*, *147*, 2582–2598. https://doi.org/10.1016/j.renene.2018.11.012

Bolund, B., Bernhoff, H., & Leijon, M. (2007). Flywheel energy and power storage systems. *Renewable and Sustainable Energy Reviews*, *11*(2), 235–258. https://doi.org/10.1016/j.rser.2005.01.004

Catolico, N., Ge, S., & McCartney, J. S. (2016). Numerical modeling of a soil–borehole thermal energy storage system. *Vadose Zone Journal*, *15*(1), 1–17. https://doi.org/10.2136/vzj2015.05.0078

Chen, H., Cong, T. N., Yang, W., Tan, C., Li, Y., & Ding, Y. (2009). Progress in electrical energy storage system: A critical review. *Progress in Natural Science*, *19*(3), 291–312. https://doi.org/10.1016/j.pnsc.2008.07.014

Cimmino, M. (2015). The effects of borehole thermal resistances and fluid flow rate on the g-functions of geothermal bore fields. *International Journal of Heat and Mass Transfer*, *91*, 1119–1127. https://doi.org/10.1016/j.ijheatmasstransfer.2015.08.041

Cimmino, M. (2018). Pygfunction: An open-source toolbox for the evaluation of thermal response factors for geothermal borehole fields. *10th Conference of IBPSA-Canada (eSIM 2018)*. https://publications.polymtl.ca/42686/

Cimmino, M. (2019). Semi-analytical method for g -function calculation of bore fields with series- and parallel-connected boreholes. *Science and Technology for the Built Environment*, *25*(8), 1007–1022. https://doi.org/10.1080/23744731.2019.1622937

Cimmino, M., & Cook, J. (2022). Pygfunction 2.2 : New features and improvements in accuracy and computational efficiency. *Proceedings of the IGSHPA Research Track 2022*. https://doi.org/10.22488/okstate.22.000015

Eskilson, P. (1987). *Thermal analysis of heat extraction boreholes. Doctoral Thesis*. University of Lund.

Hellström, G. (1991). *Ground heat storage : thermal analyses of duct storage systems. Doctoral Thesis*. University of Lund.

Kalaiselvam, S., & Parameshwaran, R. (2014). *Thermal energy storage technologies for sustainability: Systems design, assessment, and applications* [ISBN: 9780124173057]. Academic Press.

Karlsen, H., & Dong, T. (2015). A concept study for a compact high-speed rotation heat pump. In H. Selvaraj, D. Zydek, & G. Chmaj (Eds.), *Progress in systems engineering* (pp. 101–106, Vol. 366). Springer International Publishing. https://doi.org/10.1007/978-3-319-08422-0

Längauer, A., Adler, B., Rakusch, C., & Ponweiser, K. (2020). COP tests of a rotation heat pump. *25th IIR International Congress of Refrigeration (ICR 2019)*.

Lazzarotto, A. (2021). Annex 52 - Case study report for Frescati NPQ, Sweden. https://doi.org/10.23697/emqr-m785

Leidenfrost, W., & Eisele, E. H. (1972). Rotating heat exchangers and the optimization of a heat pump. *IEEE Transactions on Industry Applications*, *IA-8*(3), 345–355. https://doi.org/10.1109/TIA.1972.349766

Lemmon, E. W., Bell, I. H., Huber, M. L., & McLinden, M. O. (2018). NIST Standard Reference Database 23: Reference Fluid Thermodynamic and Transport Properties-REFPROP, Version 10.0, National Institute of Standards and Technology. https://doi.org/https://doi.org/10.18434/T4/1502528

Li, X., & Palazzolo, A. (2022). A review of flywheel energy storage systems: State of the art and opportunities. *Journal of Energy Storage*, *46*, 103576. https://doi.org/10.1016/j.est.2021.103576

Los, J., & Wind, J. (1976). *Installation equipped with a hollow rotor* (NL7607040A).

Naicker, S. S., & Rees, S. J. (2018). Performance analysis of a large geothermal heating and cooling system. *Renewable Energy*, *122*, 429–442. https://doi.org/10.1016/j.renene.2018.01.099

Naicker, S. S., & Rees, S. J. (2020). Long-term high frequency monitoring of a large borehole heat exchanger array. *Renewable Energy*, *145*, 1528–1542. https://doi.org/10.1016/j.renene.2019.07.008

Neth, F., Koenigsdorff, R., Buchmiller, D., Finkenrath, M., & Pressa, C. (2024). Modelling of seasonal borehole thermal energy storages and integration into a power plant simulation environment. *GeoTHERM Journal*, *2024*(2). https://doi.org/10.53196/gtj-2024

Nowacki, J. E., & Granryd, E. (1998). *Motor, refrigeration machine or heat pump* (WO9830846 (A1)).

Pressa, C., Jetzinger, V., Popma, H., & Finkenrath, M. (2024). Analysis of high-temperature heat pump and seasonal thermal storage integration into district heating networks. *Proceeedings of the 37th International Conference on Efficiency, Cost, Optimization, Simulation and Environmental Impact of Energy Systems*. https://doi.org/10.52202/077185

Ramstad, R. K., Justo Alonso, M., Acuña, J., Andersson, O., Stokuca, M., Håkansson, N., Midttømme, K., & Rydell, L. (2023). the borehole thermal energy storage at emmaboda, sweden: First distributed temperature measurements.

Rees, S. J. (Ed.). (2016). *Advances in ground-source heat pump systems* (Vol. number 100) [ISBN: 978-3-16-148410-0]. Woodhead Publishing.

Spitler, J., & Gehlin, S. (2019). Measured Performance of a Mixed-Use Commercial-Building Ground Source Heat Pump System in Sweden. *Energies*, *12*(10), 2020. https://doi.org/10.3390/en12102020

Štejnberg, M. O., & Idelčik, I. E. (Eds.). (2008). *Handbook of hydraulic resistance* (3. ed., 6. Jaico impr). Jaico Publ. House.

Zotter, G., Adler, B., & Längauer, A. (2024). A novel heat pumping cycle in a rotation heat pump for latent process heat supply using sensible heat sources. *16th IIR Gustav LorentzenConference on Natural Refrigerants, College Park, Maryland, USA 2024*. https://doi.org/10.18462/iir.gl2024.1113

ACKNOWLEDGEMENT

This work was funded by the German Federal Ministry for Economic Affairs and Climate Action under the funding code 03EN3073, with additional financial and in-kind support from the project partners AGFW, ecop Technologies GmbH, Fernwärme Ulm GmbH, Siemens Energy GmbH & Co. KG and ZAK Energie GmbH. The responsibility for the content of this publication lies with the authors. The authors would like to thank the funding agency and the partners for their cooperation and support during the study.